

Local Multimodal Serial Analysis for Fusing EEG-fMRI: A New Method to Study Familial Cortical Myoclonic Tremor and Epilepsy

Li Dong, Pu Wang, Yi Bin, Jiayan Deng, Yongjie Li, Leiting Chen, Cheng Luo, and Dezhong Yao

Abstract—Integrating information of neuroimaging modalities, such as electroencephalography (EEG) and functional magnetic resonance imaging (fMRI), has become popularly for investigating various types of epilepsy. However, there are also some problems for the analysis of simultaneous EEG-fMRI data in epilepsy: one is the variation of HRFs, and another is low signal-to-noise ratio (SNR) in the data. Here, we propose a new multimodal unsupervised method, termed local multimodal serial analysis (LMSA), which may compensate for these deficiencies in multimodal integration. A simulation study with comparison to the traditional EEG-informed fMRI analysis which directly implemented the general linear model (GLM) was conducted to confirm the superior performance of LMSA. Then, applied to the simultaneous EEG-fMRI data of familial cortical myoclonic tremor and epilepsy (FCMTE), some meaningful information of BOLD changes related to the EEG discharges, such as the cerebellum and frontal lobe (especially in the inferior frontal gyrus), were found using LMSA. These results demonstrate that LMSA is a promising technique for exploring various data to provide integrated information that will further our understanding of brain dysfunction.

Index Terms—Familial cortical myoclonic tremor and epilepsy (FCMTE), local multimodal serial analysis (LMSA), multimodal fusion, simultaneous EEG-fMRI.

I. INTRODUCTION

INTEGRATING information of neuroimaging modalities that can alleviate limitations of a single modality has become increasingly popular for neuroscience research and clinical application [1]. In view of their noninvasiveness and complementarity of spatiotemporal resolution, electroencephalography (EEG) and functional magnetic resonance

imaging (fMRI), have been widely integrated for investigating human brain function and dysfunction, and various multimodal methods based on EEG and fMRI have been developed [2], [3]. In general, there are three most influential approaches for EEG-fMRI fusion. (1) fMRI-informed EEG analysis: fMRI spatial information with high spatial resolution assists the inverse problem of EEG source reconstruction [4], [5]. (2) EEG-informed fMRI analysis: being implemented through a general linear model (GLM), suitable EEG features (with high temporal resolution), such as ERP amplitudes [6], the power spectrum [7], and epileptic spikes [8], assists in detecting the blood oxygen level-dependent (BOLD) changes in fMRI. This strategy is widely utilized for event-free or event conditions during simultaneous EEG-fMRI recording. (3) symmetric EEG-fMRI analysis: EEG and fMRI data are jointly integrated through a common generative model [9] or in a common data/feature space [10], [11]. In brief, the first two approaches emphasize the benefits from the strength of another modality, and the third approach emphasizes the common information while avoiding a bias of either.

Considering the scalp EEG is an effective technique for observing epileptic discharges and fMRI allows measurement of BOLD changes related epileptic discharges in the brain with high spatial resolution, combining EEG-fMRI has been popularly applied in various types of epilepsy, and the approach of EEG-informed fMRI analysis is traditional method to analyze simultaneous EEG-fMRI in epilepsy [12], [13]. In this approach, the epileptic discharges are first marked from artifact removed EEG data. And then, onset times of discharges which are convolved with a conventional hemodynamic response function (HRF) are implemented in the GLM to detect the voxels related to the EEG discharges in fMRI. The EEG informed-fMRI analysis approach has been demonstrated its ability to localize epileptic foci which providing complementary information in epilepsy, such as the focal epilepsy [14], [15] and the idiopathic generalized epilepsy [16]. However, there are also some problems for the analysis of EEG-fMRI data using GLM in epilepsy. One is the choice of the HRF in creating the model. Masterton *et al.*, have been found that canonical HRF may not provide the best model for the BOLD changes related to spikes [17]. And a compensatory strategy is using various HRFs to detect BOLD changes related with epileptic discharges [18], [19]. Another problem is that while the noise level of the simultaneous EEG (e.g., gradient artifact and ballistocardiogram artifacts) and fMRI data [high-resolution fMRI has an intrinsically lower signal-to-noise ratio (SNR) [20]] acquisition was high, the

Manuscript received October 09, 2014; revised February 03, 2015; accepted March 06, 2015. Date of publication March 10, 2015; date of current version December 09, 2015. This work was supported by the 973 project (2011CB707803), the National Nature Science Foundation of China (grant number: 91232725, 81271547, 81371636, and 81330032), the 111 project (B12027) and the Program for Changjiang Scholars and Innovative Research Team (IRT0910).

L. Dong, P. Wang, Y. Bin, J. Deng, Y. Li, L. Chen, C. Luo, and D. Yao are with the Key Laboratory for NeuroInformation of Ministry of Education, Center for Information in BioMedicine, High-Field Magnetic Resonance Brain Imaging Key Laboratory of Sichuan Province, School of Life Science and Technology, University of Electronic Science and Technology of China, Chengdu, 610054, China (e-mail: dyao@uestc.edu.cn; chengluo@uestc.edu.cn)

P. Wang is with the Department of Neurology, Sichuan Provincial People's Hospital Branch of Chongzhou and Chongzhou People's Hospital, Chongzhou, Sichuan, China.

This article has supplementary downloadable multimedia material available at <http://ieeexplore.ieee.org> provided by the authors. This includes Fig. S1, and Tables S1 and S2. This material is 1 MB in size.

Color versions of one or more of the figures in this paper are available online at <http://ieeexplore.ieee.org>.

Digital Object Identifier 10.1109/TAMD.2015.2411740

simple GLM may be difficult to uncover the fMRI weak neural signals in epilepsy [8], especially in the epilepsy of few epileptic discharges. Therefore, a more flexible and sensitive multimodal method that performs well in analyzing and exploring BOLD changes related with epileptic discharges is expected.

Familial cortical myoclonic tremor and epilepsy (FCMTE), which is characterized by a myoclonus of the extremities, tremor, infrequent epileptic seizures and nonprogressive diseases, has been reported and investigated since 1980s in Japan [21], [22]. As a rare autosomal inheritance syndrome, FCMTE have been reported only in about 70 families around the world [23], and currently only one candidate causative gene, *CNTN2*, has been identified in autosomal recessive FCMTE [24]. Abnormalities in the sensorimotor cortex, subcortical areas and cerebellum have been found in various histological [25], [26], structural [27] and functional [28], [29] studies. Thus far, the pathophysiologic mechanism of FCMTE remains speculative. Compared to the role of single modality in epilepsy studies [30], [31], multimodal methods perhaps promise to provide further functional complementary information and insight into our understanding of FCMTE.

In this paper, in view of emphasizing common substrate of modalities, decreasing uncertainty in fusion of EEG-fMRI [32] and compensating for the aforementioned deficiencies, we present a new method, termed local multimodal serial analysis (LMSA), to detect the potential BOLD changes related with EEG features. The paper is organized as follows. The mathematical theory of LMSA is described in the next section in detail. Then, the performance of LMSA is demonstrated by means of one simulation, and an example of real simultaneous EEG-fMRI data of FCMTE patients. Finally, discussions are provided regarding the performance of the method and the resultant BOLD changes in FCMTE.

II. METHOD AND MATERIALS

A. Local Multimodal Serial Analysis

Here, we demonstrate a new method that is serially fusing EEG and fMRI in the local region to efficiently capture the potential brain functional activities. This method is called the local multimodal serial analysis.

As an example, we are formally considering the two following multimodal data, EEG, and fMRI data (Fig. 1). For fMRI data, $\mathbf{Y} \in R^{M \times N}$ where M is the number of time points and N is the number of voxels, time courses of i th voxel $y_i \in R^{M \times 1}$ and its neighboring voxels (26 voxels) can be defined as matrix \mathbf{Y}_i . For EEG data, the lagged discharge function matrix, \mathbf{X} (also named lagged matrix which contains the onset times related to the epileptic discharges and downsampled to fMRI time scale), can be given as

$$\mathbf{X} = \begin{bmatrix} x_1 & 0 & \cdots & 0 \\ x_2 & x_1 & \cdots & 0 \\ \vdots & \vdots & \ddots & \vdots \\ x_k & x_{k-1} & \cdots & x_1 \\ \vdots & \vdots & \vdots & \vdots \\ x_M & x_{M-1} & \cdots & x_{M-k+1} \end{bmatrix} \quad (1)$$

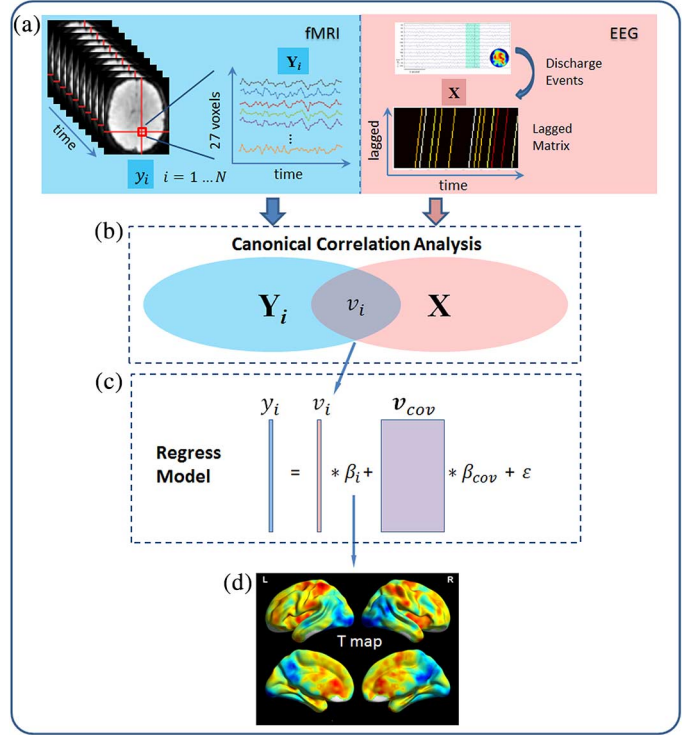


Fig. 1. The framework of local multimodal serial analysis. (a) Time courses of i th voxel and its neighboring 26 voxels, Y_i are obtained from fMRI data, and the lagged function matrix of discharge onsets X is also obtained from EEG data. (b) Canonical correlation analysis is utilized to obtain the canonical variate (v_i) which is corresponding to the maximal correlation between EEG and fMRI data sets. (c) The activity intensity (β_i) is estimated by the multiple linear regress model where v_{cov} are nuisance covariates such as head motion and linear trend signals during fMRI recording. (d) The aforementioned procedure is performed for the whole brain, and the T-map of estimated β_i can be finally obtained.

where M is the number of time points which is matched to fMRI data, and k is the number of the lagged time points. First, the maximal correlations between these two data sets, \mathbf{Y}_i and \mathbf{X} , can be solved by canonical correlation analysis, which finds the matrices of weights \mathbf{a} and \mathbf{b} such that the linear combinations $\mathbf{Y}_i * \mathbf{a}$ and $\mathbf{X} * \mathbf{b}$ maximize the pair-wise correlations across the two data sets, that is

$$\begin{aligned} & \underset{\mathbf{a}, \mathbf{b}}{\text{maximize}} \text{Corr}_{\mathbf{Y}_i * \mathbf{a}, \mathbf{X} * \mathbf{b}} \\ & \text{subject to } \text{var}(\mathbf{Y}_i * \mathbf{a}) = \text{var}(\mathbf{X} * \mathbf{b}) = 1 \end{aligned} \quad (2)$$

where $\text{var}(\cdot)$ is the variance and $\text{Corr}(\cdot, \cdot)$ is Pearson correlation. Then, the significant canonical variate $v_i = \mathbf{X} * \pm \mathbf{b}_1$ (v_i and \mathbf{b}_1 is column vector, and the sign \pm is determined by sign of maximal absolute value in \mathbf{b}_1) which is corresponding to the maximal canonical correlation coefficient, is obtained. The HRF in the local region is also estimated by weight $\pm \mathbf{b}_1$. Next, a multiple linear regress model is utilized to estimate the activity of the voxel i , that is

$$y_i = [v_i \ \mathbf{v}_{cov}] * [\beta_i \ \beta_{cov}] + \epsilon \quad (3)$$

where β_i (i th element) and β_{cov} (column vector) are the regression coefficients, v_i is canonical variate related to the maximal correlation between EEG and fMRI data sets, \mathbf{v}_{cov} is nuisance covariate matrix contained headmotion and linear trend signals

TABLE I
DETAILED DEMOGRAPHIC INFORMATION AND CLINICAL CHARACTERISTICS OF FCMTE

FCMTE Patients	Sex/Age (years)	Seizures type/onset (year)	Tremor onset (year)	Seizure frequency	Medication	24h-video EEG
#1	Male /63	GTCS/38	31	+	–	Sparse spikes with left frontal lobe predominance.
#2	Male /46	GTCS/45	22	++	–	Burst of theta sharply waves over bilaterally frontocentral lobe.
#3	Male /66	GTCS/39	35	++	VPA	Burst of theta waves in the right parietal frontal lobe.
#4	Male /69	GTCS/36	33	++	VPA/CBZ	Widespread paroxysmal spikes in the left frontoparietal region.
#5	Male /63	GTCS/48	40	+	–	Runs of diffuse theta waves.
#6	Male /48	GTCS/28	20	+	VPA	Irregular EEG.
#7	Male /46	GTCS/38	32	+	–	Bilaterally burst of theta sharply waves Right > Left.

CBZ: carbamazepine, VPA: valproic acid, GTCS: generalized tonic-clonic seizures, +: few seizures per lifetime and good control with medication ++: present few seizures per year on medication.

during fMRI recording, and ε is residual error. And, the regression coefficient β_i which represents the activity intensity of voxel i can be estimated by the following:

$$[\hat{\beta}_i \hat{\beta}_{cov}] = [v_i \mathbf{v}_{cov}]^+ * y_i \quad (4)$$

where $[\cdot]^+$ is the pseudoinverse operator. Finally, the aforementioned procedure is performed for all voxels, and the T-map of all estimated regression coefficients $\hat{\beta} \in R^{N \times 1}$ can be calculated by

$$T = \frac{\hat{\beta}}{SE(\hat{\beta})} \quad (5)$$

where $SE(\cdot)$ is standard error corresponding to $\hat{\beta}$.

B. Simulation

To illustrate the performance of the aforementioned method, a simulation that consisted of a 2D fMRI map of 5×5 grey matter voxels (a local region of one slice) was designed. For simulation of epileptic discharges, because the generating of epileptic waves is not focus in the study, 30 discharge events were random occurred in one run, and the lagged discharge function matrix X was assumed to be directly obtained. In one simulated run, 25 time courses (250 points) were generated by convolving 30 epileptic discharge events with hemodynamic response function (HRF). The TR (2 s), 3 conventional hemodynamic response functions (HRFs) of different onset times (0 TR, 1.5 TR, and 3 TR corresponding to HRF-1, HRF-2, and HRF-3) and 1 negative HRF (HRF-4) were used to generate fMRI data. Independent Gaussian noises were added in the simulation data, and SNR was set at 0.1 which is consistent with typical experimental data. Furthermore, to assess the performance of LMSA, traditional EEG-informed fMRI analysis which was implemented by GLM (convolved with conventional HRF, HRF-1) was considered in the simulation, and the different SNRs (SNR = 20, 10, 1, 0.5, 0.2, 0.1, 0.05, 0.001) were also set in the simulation. In addition, the whole simulation process was repeated 50 times, and the mean of the results is reported.

C. Real EEG-fMRI Data

Subjects: Seven male FCMTE patients (mean age: 57 yr, age range: 46–69 yr) from a Chinese FCMTE genealogy showing autosomal dominant inheritance and linkage to 8q23.3–24.13 were investigated in this study. All of patients had cortical myoclonic tremor in the upper limbs and rare generalized tonic-clonic seizures (GTCS). The EEG showed the burst of sharp theta waves or intermixed epileptiform activity when being underwent a 24 h-video EEG. The detailed demographic information and clinical characteristics of subjects were summarized in Table I. The family tree of FCMTE patients can be seen in the Fig. S1 in the supplementary materials. All of patients were signed the written informed consent. The study was approved by the Ethics Committee of the University of Electronic Science and Technology of China.

Simultaneous EEG-fMRI Recording: EEG data were recorded using a 64-channel MR compatible EEG system (NeuroScan, Charlotte, NC, USA). The EEG cap consisted of 62 scalp electrodes (Ag/AgCl ring electrodes with built-in 5 k Ω resistors) distributed according to 10-20 cap system and two additional electrodes, one placed below the left eye and the other attached below the clavicle (about 4 cm) for electrocardiogram (ECG) recording. The data were referenced to the vertex, and sampling rate was set at 5000 Hz (a low-pass filtered at 2000 Hz).

The fMRI data were recorded using a 3-T scanner (Discovery MR750, GE, USA). T1-weighted images were acquired using a three-dimensional fast spoiled gradient echo (3D-FSPGR) sequence. Generating 152 axial slices, the imaging parameters were as follows: TR/TE = 5.936 ms/1.956 ms, flip angle = 9 $^\circ$, field of view = 256 \times 256 mm 2 , voxel size = 1 \times 1 \times 1 mm 3 , slice thickness (no gap) = 1 mm. Functional images were collected using a gradient-echo echo-planar imaging (EPI) sequence, and the imaging parameters were as follows: TR/TE = 2000 ms/30 ms, flip angle = 90 $^\circ$, matrix size = 64 \times 64, field of view = 240 \times 240 mm 2 , slice thickness = 4 mm. A total number of 255 volumes (35 slices per volumes) were obtained over a run period (510 s), and all functional images were obtained from five repeated runs (a total of 40.25

TABLE II
THE SUMMARY OF SIGNIFICANT BOLD CHANGES RELATED TO DISCHARGES UNCOVERED BY LMSA

	Number of discharges (TR)	Regions of BOLD changes related to the discharges							
		Cerebellum	Inferior Frontal Gyrus	Occipital Lobe	Sensorimotor Cortex	Temporal Lobe	Cingulate Gyrus	Basal Ganglia	Thalamus
		Patient #1	51	–	↑ R	↓ R	↑ L	↑ L	↑ B
Patient #2	8	↓ B	↓ B	↓ R	↓ L	–	–	↓ B	↓ B
Patient #3	55	↓ B	↓ B	↑ R	–	↓ B	↓ B	–	↓ R
Patient #4	6	↓ L	↑ R	–	↑ B	↑ B	–	–	–
Patient #5	31	↓ B; ↑ B	↑ B	↑ B	↑ B	↑ B	↑ B	↓ B	–
Patient #6	15	↑ B	↑ L	↑ L	↑ L	↓ L; ↑ R	↑ B	–	–
Patient #7	81	↓ B; ↑ B	↓ L; ↑ R	↓ R; ↑ L	↑ B	↑ B	↑ B	↑ B	–

↑: activation; ↓: deactivation; B: bilateral; L: left; R: right.

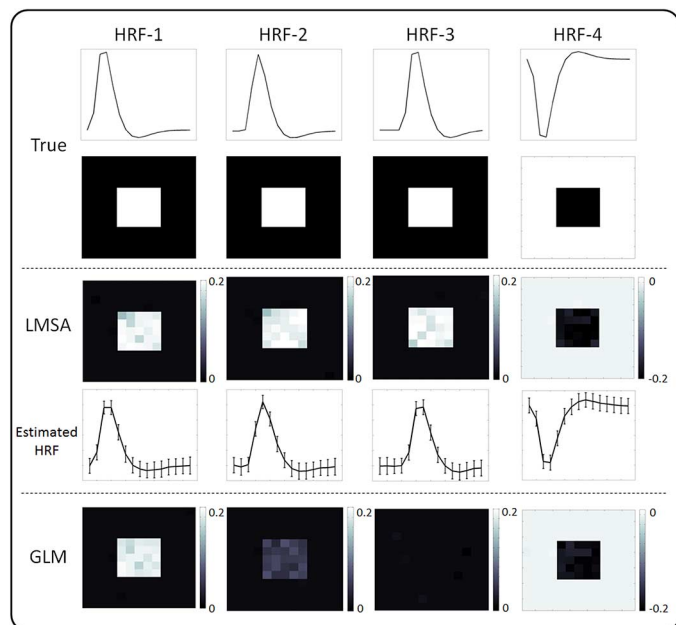


Fig. 2. The mean results of simulation. The first row illustrates the various shapes of HRFs, and the second row shows the true situations of neural positive (first column to third column) and negative (fourth column) activity. Mean regression coefficients of LMSA (third row), estimated HRFs of LMSA (mean and standard deviation, fourth row) and GLM (fifth row) are also showed.

min). During scanning, all patients were instructed to close their eyes and relax without falling asleep.

Real Data Processing: EEG data of all runs were primarily analyzed using the Curry 7 (NeuroScan software). All EEG data were re-referenced to the common average reference, then analyzed. Briefly, gradient artifacts were removed using a local average artifact template procedure [33] while a moving average width of 15 MR volumes was used. In addition, the EEG data were 1–30-Hz passband filtered and downsampled to 250 Hz. Next, most of the ballistocardiogram (BCG) artifacts were removed using the OBS-based BCG correction [34]. Then, the onset times of epileptic discharges were independently identified by two experienced neurologists with the best agreement.

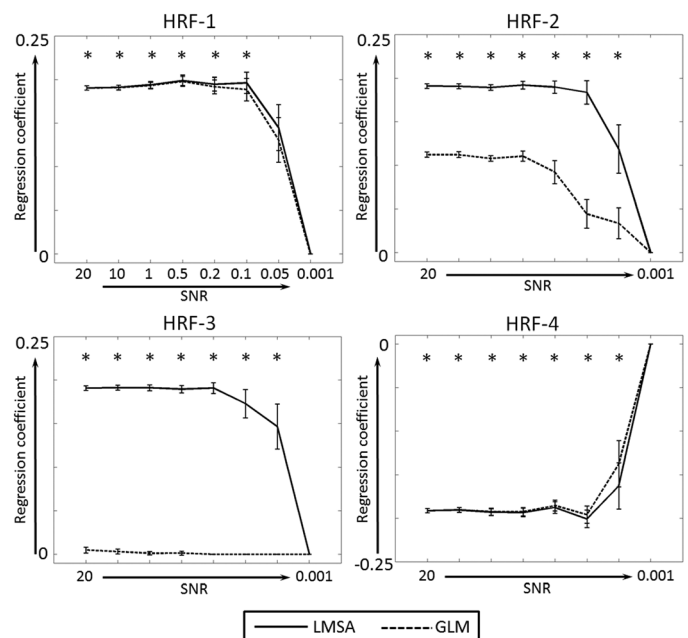


Fig. 3. The performances of LMSA and GLM using simulation data with different SNRs (from 20 to 0.001). Mean regression coefficients (with standard error) of the center voxel (one voxel) estimated by LMSA and GLM with various HRFs and SNRs are showed. SNR: signal-to-noise ratio. *: significant ($P < 0.05$).

Runs were excluded if the number of epileptic discharges less than 5 TR time points during simultaneous fMRI scanning.

The first five volumes were first discarded to remove the T1 saturation effects. Slice time correction, realignment, spatial normalization ($3 \times 3 \times 3 \text{ mm}^3$) and spatial smoothing (8 mm full-width at half-maximum of an isotropic Gaussian filter) were conducted by SPM8 (<http://www.fil.ion.ucl.ac.uk/spm>). Runs were excluded if head motion exceeded 1.5 mm (translation) and 1.5° (rotation) during fMRI acquisition.

In this paper, onsets of epileptic discharge obtained from EEG data and preprocessed fMRI data were finally analyzed with aforementioned LMSA procedures. To assess the performance of LMSA, traditional EEG-informed fMRI analysis (GLM involved with conventional HRF) was also conducted.

III. RESULTS

A. Simulation Results

In the simulation, three positive HRFs of different onset times (0 TR, 1.5 TR, and 3 TR) and 1 negative HRF were first considered, and the SNR was set at 0.1. Fig. 2 shows the mean values ($P < 0.001$) of regression coefficients estimated by LMSA (the lagged time points, k , was set at 15) and GLM (using standard HRF, i.e., HRF-1). LMSA accurately detected the all assumed neural activities which convolved with various HRFs, but also had ideal ability to distinguish between the true activities and stochastic disturbance. As a core procedure of traditional EEG-informed fMRI analysis, GLM could accurately uncover the assumed activities while using appropriate HRFs (using HRF-1 while the true HRFs are HRF-1 and HRF-4). However, in the case of convolving with unfitting HRFs (using HRF-1 while the true HRFs are HRF-2 and HRF-3), GLM obviously produced decreased coefficients, even did not capture the potential neural activities. To assess the effects of the noise, different noise levels (SNR = 20, 10, 1, 0.5, 0.2, 0.1, 0.05, and 0.001) were also considered; the mean results of these simulations (in the center voxel) are depicted in Fig. 3. Regression coefficients estimated by GLM and LMSA were trending to zero 0 with increasing noise, however, LMSA performed better than GLM for detecting potential activities (paired t test, $P < 0.05$). In detail, for the HRF-1 and HRF-4, LMSA and GLM had similar performances of uncovering neural activities with high SNR level. For the HRF-2, LMSA produced higher coefficients than GLM with all SNR levels ($P < 10^{-16}$ for SNR = 20, 10, 1, 0.5, 0.2 and 0.1, $P < 10^{-4}$ for SNR = 0.05). For the HRF-3, GLM did not capture the assumed activities at all SNR levels, but LMSA produced appropriate coefficients for uncovering the potential activities ($P < 10^{-11}$ for all SNRs).

B. Real Data Results

For the real simultaneous EEG-fMRI data, an example of 8 Hz sharp waves (PZ, P4, CP4, P7, P3, and CP3) in patient #7 is showed in Fig. 4. The significant BOLD changes ($P < 0.001$, uncorrected, voxel size $> 621 \text{ mm}^3$) related to the EEG discharges revealed by LMSA (the lagged time points, k , was set at 10) in FCMTE patients contained the cerebellum, inferior frontal gyrus, occipital lobe and sensorimotor cortex (Table II). And, the details of results of LMSA and GLM (also using standard HRF, i.e., HRF-1) were present as follows (see Fig. 5, Table S1, and Table S2).

Patient #1:

The activation regions uncovered by LMSA consisted of the left precentral gyrus [Brodmann Area (BA) 3], bilateral anterior cingulate (BA32/BA24), bilateral insula (BA13) and right inferior frontal gyrus (BA9). The deactivation regions revealed by LMSA encompassed the bilateral occipital lobe (BA18), precuneus (BA31/BA23) and right angular gyrus (BA40). For GLM, only the activations were found in the bilateral insula (BA13), supplementary motor area (BA6), precentral gyrus (BA6), and inferior frontal gyrus (BA47).

Patient #2:

For LMSA, main activation regions consisted of the bilateral basal ganglia, bilateral inferior frontal gyrus (BA9/BA46), left supplementary motor area (BA6), left precentral gyrus (BA6), right occipital lobe (BA18) and bilateral cerebellum posterior lobe. And for GLM, only the deactivation in the bilateral caudate was found.

Patient #3:

The activations uncovered by LMSA were in the right cuneus (BA18), and the deactivation regions encompassed the bilateral cerebellum posterior lobe, bilateral middle temporal gyrus (BA21), bilateral superior frontal gyrus (BA9/BA9/BA10), bilateral middle cingulate gyrus (BA32), bilateral inferior frontal gyrus (BA45), and right thalamus. However, there were no regions revealed by GLM.

Patient #4:

The activations in the right inferior frontal gyrus (BA44), bilateral precentral gyrus (BA6), right superior frontal gyrus (BA10), bilateral temporal pole (BA38), and middle temporal gyrus (BA21), and deactivation in the left cerebellum posterior lobe were found by LMSA. For GLM, the activations in the bilateral precuneus (BA7), superior frontal gyrus (BA10), supplementary motor area (BA6), middle temporal gyrus (BA21), left inferior frontal gyrus (BA47), and left middle occipital gyrus (BA37) were revealed.

Patient #5:

The main activations in the bilateral middle frontal gyrus (BA10), precentral gyrus (BA48), occipital lobe (BA19), paracentral lobule (BA6), cerebellum posterior lobe and middle frontal gyrus (BA8/BA10) were found by LMSA, and the deactivation was found in the bilateral putamen. There were no regions uncovered by GLM.

Patient #6:

For LMSA, the main activation regions consisted of the left inferior frontal gyrus (BA47/BA11), left occipital lobe (BA18), bilateral cerebellum anterior lobe, left postcentral gyrus (BA6/BA4), bilateral fusiform gyrus (BA20) and right superior temporal gyrus (BA42), and the deactivation encompassed the left inferior temporal gyrus (BA20). For GLM, only the activations in the right superior temporal gyrus (BA22), right postcentral gyrus (BA4) and left middle temporal gyrus (BA37) were found.

Patient #7:

The main activation regions revealed by LMSA encompassed the bilateral inferior parietal lobule (BA40), postcentral gyrus (BA43), cingulate gyrus (BA23/BA32), right orbitofrontal area (BA11) and bilateral cerebellum anterior lobe, and the deactivation regions contained the bilateral cerebellum posterior lobe, right middle temporal gyrus (BA37), right middle occipital gyrus (BA19), left posterior cingulate (BA29) and left middle frontal gyrus (BA6/BA8). For GLM, only the activation in the left anterior cingulate (BA32) and the deactivation in the right middle frontal gyrus (BA11) were found.

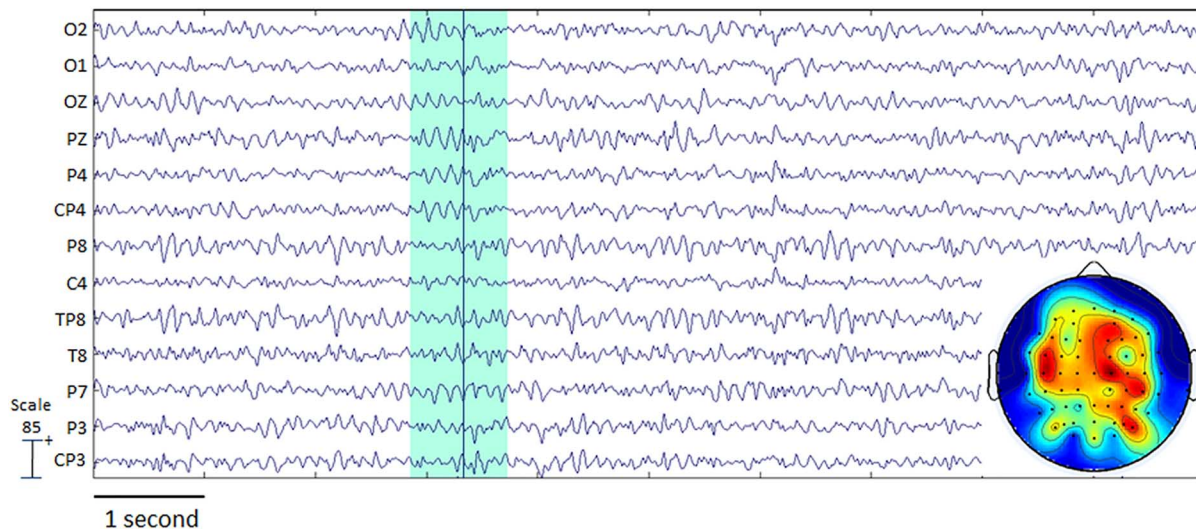


Fig. 4. The EEG of patient #7. An example of 8 Hz sharp waves in the PZ, P4, CP4, P7, P3, and CP3 is shown, and the topography in one time point of discharge is also displayed.

IV. DISCUSSION AND CONCLUSION

In this paper, we proposed a new multimodal method, termed local multimodal serial analysis, for detecting the BOLD changes related to EEG features. And, performance and superiority of LMSA were investigated and illustrated in a simulation and the simultaneous EEG-fMRI data of FCMTE patients in this paper.

In the simulation, to illustrate the performance of LMSA for the various shapes of HRFs (HRF-1 to HRF-4), the Gaussian noises were initially fixed to obtain the mean results across 50 repeated calculations. For all situations of HRFs, LMSA performed well in detecting the assumed BOLD changes, while GLM could not tolerate several variably shaped HRFs due to its fixedly convolving with a conventional HRF (Fig. 2). Furthermore, although regression coefficients estimated by GLM and LMSA both were trending to zero 0 with increasing noise, however, LMSA performed better than GLM for detecting activities (Fig. 3). It is well established that HRFs vary across brain regions in the healthy subjects [35], [36] and also vary between epilepsy patients [17] or between discharges in same patient [8], and this variation may potentially lead to difficulty to detecting the neural activities. For the GLM, using various HRFs [e.g., HRFs of peaking times [19], HRFs with optimal parameters [18] and subject-specific HRFs generated from task [37]] may relax this problem, however, it is also difficult to ensure the optimal HRFs for detecting of BOLD changes related with epileptic discharges. Because of implementing canonical correlation analysis (CCA) which optimizes the mutual information between two modalities [1] and considering the EEG lagged matrix (X), freedom of LMSA is increased, and LMSA optimally emphasizes the common substrate of EEG and fMRI in local regions. Therefore, LMSA offers higher sensitivity for detecting weak changes of BOLD signals, and tolerates variably shaped HRFs. Furthermore, because CCA has low specificity (may classify nonactive voxels as active) and increased susceptibility to artifacts [38], in LMSA, canonical variates corresponding to the

EEG lagged matrix are selected as linear predictors to compensate the deficiencies of CCA. That means LMSA also decreases the uncertainty when considering the common subspace of EEG and fMRI. In brief, LMSA may achieve the objects for any fusions of two modalities should be emphasized [32]. In addition, since the definitions of two data sets (EEG lagged matrix X and local fMRI signals Y_i in our paper) in CCA are quite flexible, LMSA may have general applicability for various modalities. That is, matrix X could be EEG power spectrums, event-related potential amplitudes, or other EEG features, or for this matter any type of neuroimages (such as near-infrared spectroscopy and magnetoencephalogram), and matrix Y_i could be other types of varying parameters or even other types of neuroimages.

In the real EEG-fMRI data, the aforementioned methods (LMSA versus GLM) were utilized to detect potential BOLD changes related with EEG discharges in FCMTE patients. For the GLM, few significant BOLD changes were found in 5/7 patients, and no significant results were obtained in 2/7 patients (Fig. 5 and Table S2). For LMSA, significant BOLD changes in the cerebellum, which was reported in previous histological [25], [26], structural [27] and functional [28], [29] studies, were found in 6/7 patients (Table II and Table S1). Although the role of the cerebellum in FCMTE is also not very clear so far [22], our study provided further EEG-fMRI functional evidence that cerebellum might be related with the epileptic discharges in FCMTE. The significant BOLD changes in the frontal lobe, especially in the inferior frontal gyrus (7/7 patients, Fig. 5, Table II and Table S1), was found in FCMTE patients, and this region may be also related to the epileptic activity. In general, the frontal lobe is related with the motor control. The significantly altered BOLD signals in the inferior frontal gyrus might reflect the association with myoclonic tremor in FCMTE patients. In addition, information of BOLD changes in the frontal lobe may provide useful information for suggesting a candidate causative gene for FCMTE. BOLD changes related to discharges in the sensorimotor cortex and occipital lobe (6/7

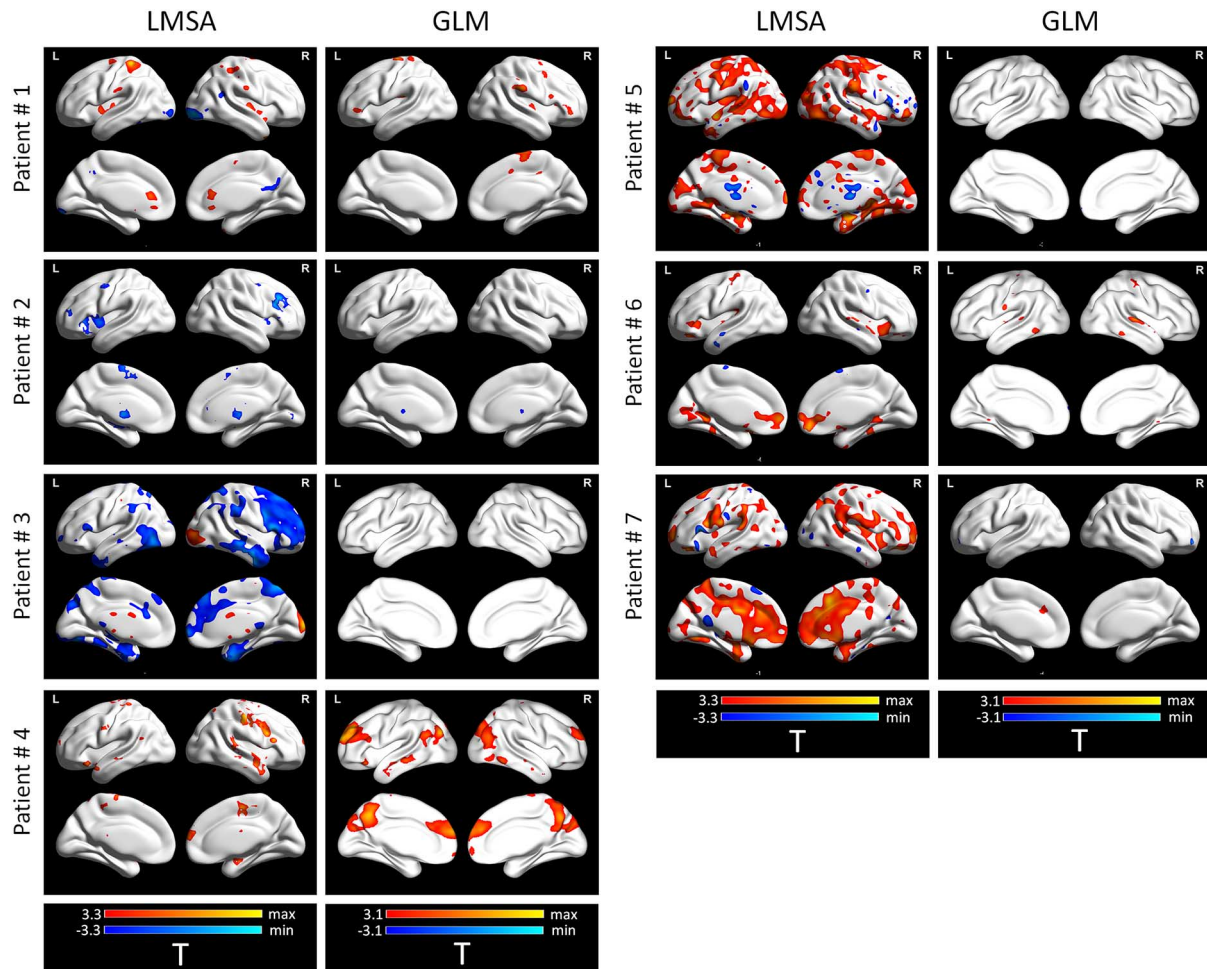


Fig. 5. Results of real EEG-fMRI data of FCMTE patients using LMSA and GLM. The significance was set at 0.001 (uncorrected, voxel size $> 621\text{mm}^3$). T: T-value; L: left; R: right.

patients, Fig. 5, Table II and Table S1) perhaps also reflect the relation with myoclonic tremor [28], [29] and visuospatial impairment [39] in FCMTE patients. The other regions detected by LMSA would implicate their contribution to investigation of epileptic network [40], [41]. In addition, the limitation of the present study was the small number of FCMTE patients in each group. However, to date, only about 70 FCMTE families have been reported [23]; our study may provide useful information for FCMTE, and also intend to increase the FCMTE patients for further analyses in the future.

In conclusion, the novelty of this paper contains that, in the process termed LMSA, we proposed a multimodal method which emphasized both the common subspaces of two modalities and decrease of the uncertainty in multimodal fusion. The simulation shows its sensitivity and superiority for detecting weak changes of BOLD signals related with EEG features. Furthermore, in simultaneous EEG-fMRI data of FCMTE patients, LMSA performed well in revealing the underlying BOLD changes related with epileptic discharges which perhaps provided important multimodal information for FCMTE. We assume that this new method may have potential for providing further integration information of various modalities that help us understand the brain dysfunction.

REFERENCES

- [1] F. Biessmann, S. Plis, F. C. Meinecke, T. Eichele, and K. R. Muller, "Analysis of multimodal neuroimaging data," *IEEE Rev. Biomed. Eng.*, vol. 4, pp. 26–58, 2011.
- [2] R. J. Huster, S. Debener, T. Eichele, and C. S. Herrmann, "Methods for simultaneous EEG-fMRI: An introductory review," *J. Neurosci.*, vol. 32, pp. 6053–60, May 2, 2012.
- [3] H. Laufs, "A personalized history of EEG-fMRI integration," *Neuroimage*, vol. 62, pp. 1056–67, Aug. 15, 2012.
- [4] W. Ou, A. Nummenmaa, J. Ahveninen, J. W. Belliveau, M. S. Hamalainen, and P. Golland, "Multimodal functional imaging using fMRI-informed regional EEG/MEG source estimation," *Neuroimage*, vol. 52, pp. 97–108, Aug. 1, 2010.
- [5] X. Lei, P. Xu, C. Luo, J. Zhao, D. Zhou, and D. Yao, "fMRI functional networks for EEG source imaging," *Hum. Brain Mapp.*, vol. 32, pp. 1141–60, Jul. 2011.
- [6] S. Debener, M. Ullsperger, M. Siegel, K. Fiehler, D. Y. von Cramon, and A. K. Engel, "Trial-by-trial coupling of concurrent electroencephalogram and functional magnetic resonance imaging identifies the dynamics of performance monitoring," *J. Neurosci.*, vol. 25, pp. 11730–7, Dec. 14, 2005.
- [7] R. Scheeringa, K. M. Petersson, R. Oostenveld, D. G. Norris, P. Hagoort, and M. C. Bastiaansen, "Trial-by-trial coupling between EEG and BOLD identifies networks related to alpha and theta EEG power increases during working memory maintenance," *Neuroimage*, vol. 44, pp. 1224–38, Feb. 1, 2009.
- [8] C. Luo, Z. Yao, Q. Li, X. Lei, D. Zhou, and Y. Qin *et al.*, "Imaging foci of epileptic discharges from simultaneous EEG and fMRI using the canonical HRF," *Epilep. Res.*, vol. 91, pp. 133–42, Oct. 2010.

- [9] K. J. Friston, L. Harrison, and W. Penny, "Dynamic causal modelling," *Neuroimage*, vol. 19, pp. 1273–302, Aug. 2003.
- [10] M. Moosmann, T. Eichele, H. Nordby, K. Hugdahl, and V. D. Calhoun, "Joint independent component analysis for simultaneous EEG-fMRI: Principle and simulation," *Int. J. Psychophysiol.*, vol. 67, pp. 212–21, Mar. 2008.
- [11] N. M. Correa, T. Adali, Y. O. Li, and V. D. Calhoun, "Canonical correlation analysis for data fusion and group inferences: Examining applications of medical imaging data," *IEEE Signal Process. Mag.*, vol. 27, pp. 39–50, 2010.
- [12] J. Gotman, "Epileptic networks studied with EEG-fMRI," *Epilepsia*, vol. 49, pp. 42–51, 2008, Suppl 3.
- [13] J. Gotman and F. Pittau, "Combining EEG and fMRI in the study of epileptic discharges," *Epilepsia*, vol. 52, pp. 38–42, Jul. 2011, Suppl 4.
- [14] R. Rathakrishnan, F. Moeller, P. Levan, F. Dubeau, and J. Gotman, "BOLD signal changes preceding negative responses in EEG-fMRI in patients with focal epilepsy," *Epilepsia*, vol. 51, pp. 1837–45, Sep. 2010.
- [15] J. Jacobs, P. Levan, F. Moeller, R. Boor, U. Stephani, and J. Gotman *et al.*, "Hemodynamic changes preceding the interictal EEG spike in patients with focal epilepsy investigated using simultaneous EEG-fMRI," *Neuroimage*, vol. 45, pp. 1220–31, May 1, 2009.
- [16] J. Gotman, C. Grova, A. Bagshaw, E. Kobayashi, Y. Aghakhani, and F. Dubeau, "Generalized epileptic discharges show thalamocortical activation and suspension of the default state of the brain," in *Proc. Natl. Acad. Sci.*, Oct. 18, 2005, vol. 102, pp. 15236–40.
- [17] R. A. Masterton, A. S. Harvey, J. S. Archer, L. M. Lillywhite, D. F. Abbott, and I. E. Scheffer *et al.*, "Focal epileptiform spikes do not show a canonical BOLD response in patients with benign rolandic epilepsy (BECTS)," *Neuroimage*, vol. 51, pp. 252–60, May 15, 2010.
- [18] F. Grouiller, L. Vercueil, A. Krainik, C. Segebarth, P. Kahane, and O. David, "Characterization of the hemodynamic modes associated with interictal epileptic activity using a deformable model-based analysis of combined EEG and functional MRI recordings," *Hum. Brain Mapp.*, vol. 31, pp. 1157–73, Aug. 2010.
- [19] A. P. Bagshaw, Y. Aghakhani, C. G. Benar, E. Kobayashi, C. Hawco, and F. Dubeau *et al.*, "EEG-fMRI of focal epileptic spikes: Analysis with multiple haemodynamic functions and comparison with gadolinium-enhanced MR angiograms," *Hum. Brain Mapp.*, vol. 22, pp. 179–92, Jul. 2004.
- [20] K. Tabelow, V. Piech, J. Polzehl, and H. U. Voss, "High-resolution fMRI: Overcoming the signal-to-noise problem," *J. Neurosci. Methods*, vol. 178, pp. 357–65, Apr. 15, 2009.
- [21] A. Ikeda, R. Kakigi, N. Funai, R. Neshige, Y. Kuroda, and H. Shibasaki, "Cortical tremor: A variant of cortical reflex myoclonus," *Neurology*, vol. 40, pp. 1561–5, Oct. 1990.
- [22] S. Sharifi, E. Aronica, J. H. Koelman, M. A. Tijssen, and A. F. Van Rootselaar, "Familial cortical myoclonic tremor with epilepsy and cerebellar changes: Description of a new pathology case and review of the literature," *Tremor Other Hyperkinet Mov (NY)*, vol. 2, 2012.
- [23] L. Licchetta, T. Pippucci, F. Bisulli, G. Cantalupo, P. Magini, and L. Alvisi *et al.*, "A novel pedigree with familial cortical myoclonic tremor and epilepsy (FCMTE): Clinical characterization, refinement of the FCMTE2 locus, and confirmation of a founder haplotype," *Epilepsia*, vol. 54, pp. 1298–306, Jul. 2013.
- [24] E. Stogmann, E. Reinthaler, S. Eltawil, M. A. El Etribi, M. Hemeda, and N. E. Nahhas *et al.*, "Autosomal recessive cortical myoclonic tremor and epilepsy: Association with a mutation in the potassium channel associated gene CNTN2," *Brain*, vol. 136, pp. 1155–60, Apr. 2013.
- [25] A. F. van Rootselaar, S. M. van der Salm, L. J. Bour, M. J. Edwards, P. Brown, and E. Aronica *et al.*, "Decreased cortical inhibition and yet cerebellar pathology in 'familial cortical myoclonic tremor with epilepsy'," *Mov. Disord.*, vol. 22, pp. 2378–85, Dec. 2007.
- [26] A. F. van Rootselaar, E. Aronica, E. N. Jansen Steur, J. M. Rozemuller-Kwakkel, R. A. de Vos, and M. A. Tijssen, "Familial cortical tremor with epilepsy and cerebellar pathological findings," *Mov. Disord.*, vol. 19, pp. 213–7, Feb. 2004.
- [27] A. W. Buijink, M. W. Caan, M. A. Tijssen, J. M. Hoogduin, N. M. Maurits, and A. F. van Rootselaar, "Decreased cerebellar fiber density in cortical myoclonic tremor but not in essential tremor," *Cerebellum*, vol. 12, pp. 199–204, Apr. 2013.
- [28] A. F. van Rootselaar, N. M. Maurits, R. Renken, J. H. Koelman, J. M. Hoogduin, and K. L. Leenders *et al.*, "Simultaneous EMG-functional MRI recordings can directly relate hyperkinetic movements to brain activity," *Hum. Brain Mapp.*, vol. 29, pp. 1430–41, Dec. 2008.
- [29] A. F. van Rootselaar, N. M. Maurits, J. H. Koelman, J. H. van der Hoeven, L. J. Bour, and K. L. Leenders *et al.*, "Coherence analysis differentiates between cortical myoclonic tremor and essential tremor," *Mov. Disord.*, vol. 21, pp. 215–22, Feb. 2006.
- [30] K. Xue, C. Luo, D. Zhang, T. Yang, J. Li, and D. Gong *et al.*, "Diffusion tensor tractography reveals disrupted structural connectivity in childhood absence epilepsy," *Epilepsy Res.*, vol. 108, pp. 125–38, Jan. 2014.
- [31] C. Luo, Q. Li, Y. Lai, Y. Xia, Y. Qin, and W. Liao *et al.*, "Altered functional connectivity in default mode network in absence epilepsy: A resting-state fMRI study," *Hum. Brain Mapp.*, vol. 32, pp. 438–49, Mar. 2011.
- [32] J. Daunizeau, H. Laufs, and K. J. Friston, "EEG-fMRI information fusion: Biophysics and data analysis," in *EEG-fMRI*. New York, NY, USA: Springer-Verlag, 2010, pp. 511–526.
- [33] P. J. Allen, O. Josephs, and R. Turner, "A method for removing imaging artifact from continuous EEG recorded during functional MRI," *Neuroimage*, vol. 12, pp. 230–9, Aug. 2000.
- [34] R. K. Niazy, C. F. Beckmann, G. D. Iannetti, J. M. Brady, and S. M. Smith, "Removal of fMRI environment artifacts from EEG data using optimal basis sets," *Neuroimage*, vol. 28, pp. 720–37, Nov. 15, 2005.
- [35] F. M. Miezin, L. Maccotta, J. M. Ollinger, S. E. Petersen, and R. L. Buckner, "Characterizing the hemodynamic response: Effects of presentation rate, sampling procedure, and the possibility of ordering brain activity based on relative timing," *Neuroimage*, vol. 11, pp. 735–59, Jun. 2000.
- [36] D. A. Handwerker, J. M. Ollinger, and M. D'Esposito, "Variation of BOLD hemodynamic responses across subjects and brain regions and their effects on statistical analyses," *Neuroimage*, vol. 21, pp. 1639–51, Apr. 2004.
- [37] S. Proulx, M. Safi-Harb, P. Le Van, D. An, S. Watanabe, and J. Gotman, "Increased sensitivity of fast BOLD fMRI with a subject-specific hemodynamic response function and application to epilepsy," *Neuroimage*, Feb. 25, 2014.
- [38] R. Nandy and D. Cordes, "Improving the spatial specificity of canonical correlation analysis in fMRI," *Magn. Reson. Med.*, vol. 52, pp. 947–52, Oct. 2004.
- [39] A. Suppa, A. Berardelli, F. Brancati, M. Marianetti, G. Barrano, and C. Mina *et al.*, "Clinical, neuropsychological, neurophysiologic, and genetic features of a new Italian pedigree with familial cortical myoclonic tremor with epilepsy," *Epilepsia*, vol. 50, pp. 1284–8, May 2009.
- [40] H. Laufs, "Functional imaging of seizures and epilepsy: Evolution from zones to networks," *Curr. Opin. Neurol.*, vol. 25, pp. 194–200, Apr. 2012.
- [41] C. Luo, D. An, D. Yao, and J. Gotman, "Patient-specific connectivity pattern of epileptic network in frontal lobe epilepsy," *Neuroimage Clin.*, vol. 4, pp. 668–75, 2014.



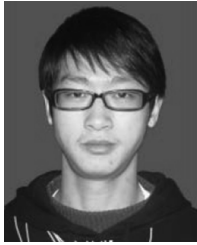
Li Dong was born in Chongqing, China, 1988. He received the B.S. degree in mathematics and applied mathematics from the Beijing Institute of Technology, Beijing, China, in 2009.

Since 2010, he is a Ph.D. degree candidate in biomedical engineering, School of Life Science and Technology, University of Electronic Science and Technology of China, Chengdu, China. His current research interests include functional connectivity and spatiotemporal features of the brain in fMRI (resting state), brain network and its topological property, EEG-fMRI multimodal integration, and also the application for the neuropsychiatric disorder (e.g., epilepsy) and cognitive science.



Pu Wang received the M.S. degree in neurology from Luzhou Medical College in 2012.

She is the attending doctor at the Department of Neurology, Sichuan Provincial People's Hospital Branch of Chongzhou and Chongzhou People's Hospital, Chongzhou, Sichuan, China. Her current research interests include resting state functional connectivity and imaging genetics of epilepsy.



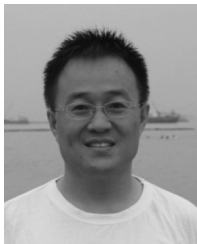
Yi Bin received the B.S. degree from the Civil Aviation University of China in 2013.

He then joined the Key Laboratory for NeuroInformation of Ministry of Education in 2014, as a postgraduate in the School of Life Science and Technology, University of Electronic Science and Technology of China. His research interests include brain network and AI.



Jia-yan Deng received the B.S. degree in biomedical engineering from North Sichuan Medical College in 2013.

Now, she also pursues her graduate work in biomedical engineering at the University of Electronic Science and Technology of China. Her research interests include applications of fMRI in epilepsy and Parkinson's disease.



Yong-Jie Li (M'XX) received the Ph.D. degree in biomedical engineering from the University of Electronic Science and Technology of China (UESTC), Chengdu, China, in 2004.

He is currently a Professor with the Key Laboratory for Neuroinformation, Ministry of Education, School of Life Science and Technology, UESTC, China. His research interests include visual mechanism modeling, image processing, and brain-like computation.



Lei-ting Chen (M'XX) was born in Taiyuan City, Shanxi Province, China, in 1966. He received the B.S. degrees in information system engineering from Northwestern Polytechnical University, Xi'an, Shanxi, China, in 1987, the M.S. degree in computer software from the University of Electronic Science and Technology of China (UESTC), Chengdu, Sichuan, China, in 1994, and the Ph.D. degree in computer application technology from the UESTC in 2007.

From 1994 to 1999, he was an Assistant Professor with the Microcomputer Institute, UESTC. From 1999 to 2005, he was an As-

sociate Professor with School of Computer Science and Engineering, UESTC. Since 2005, he has been a Full Professor with School of Computer Science and Engineering, UESTC, and the Director of the Key Laboratory for Virtual Reality Technology of Ministry of Information Industry of China. Since 2010, he has become the Director of the Key Laboratory for Digital Media Technology of Sichuan Province, and joined the Key Laboratory for NeuroInformation of Ministry of Education (UESTC) in 2013. He is the author of three books, more than 150 articles, more than 40 inventions, and holds 16 patents. His research interests include digital medical image processing, computer graphics, virtual reality, digital media.

Dr. Chen is a member of editorial board of the *Journal of Computer Applications*. Since 2009, he has been a member of IET and ACM. He won a Second Class Prize of the National Scientific and Technological Progress Award of China in 2011.



Cheng Luo received the Ph.D. degree in biomedical engineering from University of Electronic Science and Technology of China (UESTC), Chengdu, China, in 2011.

Between 2012 and 2013, he was a Postdoctoral Fellow at the Montreal Neurological Institute, McGill University, Montreal, Canada, working on epileptic functional connectivity based on EEG-fMRI. He is currently with the Key Laboratory for NeuroInformation of Ministry of Education, School of Life Science and Technology, UESTC, as an Associate Professor. His current research focuses on the functional and structural connectivity study in epilepsy, schizophrenia, and aging.



De-Zhong Yao was born in Chongqing, China, 1965. He received the Ph.D. degree in applied geophysics from the Chengdu University of Technology, Chengdu, China, in 1991, and completed his postdoctoral fellowship in electromagnetic field with UESTC in 1993.

He has been a faculty member since 1993, a professor since 1995, and the Dean of the School of Life Science and Technology, UESTC, since 2001; as well as Director of the Key Laboratory for NeuroInformation of Ministry of Education, since 2009. He was a visiting scholar with the University of Illinois at Chicago, IL, USA, from September 1997 to August 1998, and a visiting professor with McMaster University, Canada, from November 2000 to May 2001 and with Aalborg University, Denmark, from November 2003 to February 2004. He has published more than 100 peer reviewed papers in international journals and conferences. His current research interests include EEG and fMRI with their applications in cognitive science and neurological problems.